Solar Phys (2010) 261: 53–75
DOI 10.1007/s11207-009-9475-x

# The Structure and Dynamics of the Upper Chromosphere and Lower Transition Region as Revealed by the Subarcsecond VAULT Observations

**A. Vourlidas · B. Sanchez Andrade-Nuño · E. Landi · S. Patsourakos · L. Teriaca · U. Schühle · C.M. Korendyke · I. Nestoras**

Received: 9 September 2009 / Accepted: 20 October 2009 / Published online: 15 December 2009


**Abstract** The Very high Angular resolution ULtraviolet Telescope (VAULT) is a sounding rocket payload built to study the crucial interface between the solar chromosphere and the corona by observing the strongest line in the solar spectrum, the Ly α line at 1216 Å. In two flights, VAULT succeeded in obtaining the first ever subarcsecond (0.5″) images of this region with high sensitivity and cadence. Detailed analyses of those observations contributed significantly to new ideas about the nature of the transition region. Here, we present a broad overview of the Ly α atmosphere as revealed by the VAULT observations and bring together past results and new analyses from the second VAULT flight to create a synthesis of our current knowledge of the high-resolution Ly α Sun. We hope that this work will serve as a good reference for the design of upcoming Ly α telescopes and observing plans.

**Keywords** Line: hydrogen Ly alpha atomic data · Sun: corona · Sun: UV radiation · Sun: transition region

A. Vourlidas (✉) · B. Sanchez Andrade-Nuño · E. Landi · C.M. Korendyke
Space Science Division, Naval Research Laboratory, 4555 Overlook Ave, SW, Washington, DC, USA
e-mail: vourlidas@nrl.navy.mil

B. Sanchez Andrade-Nuño
e-mail: bsanchez@ssd5.nrl.navy.mil

B. Sanchez Andrade-Nuño · S. Patsourakos
George Mason University, 4400 University Dr, Fairfax, VA, USA

L. Teriaca · U. Schühle
MPI for Solar System Research, 37191 Katlenburg-Lindau, Germany

L. Teriaca
e-mail: teriaca@mps.mpg.de

U. Schühle
e-mail: schuele@mps.mpg.de

I. Nestoras
Max-Plank-Institut für Radioastronomie, Auf dem Hügel 69, 53121 Bonn, Germany

## 1. Introduction

The structure of the solar atmosphere as a function of temperature was a "thorny" issue of solar physics research for decades. As the density decreases, the temperature, instead of decreasing, abruptly increases from $\sim 10^4$ K to 1 000 000 K within 1000 km. It is known from the first solar imaging space missions that this so-called temperature transition region (TR) between the chromosphere and the corona is also where the morphology of the atmospheric structures changes strongly. At the base of the atmosphere, the photosphere consists of small-scale convective granules interlaced with occasional smaller intergranular lanes concentrating strong magnetic flux elements ($|B| \leq 1kG$, *e.g.*, Trujillo Bueno, Shchukina, and Asensio Ramos, 2004). The chromosphere ($T \leq 10^4$ K for the discussion here) consists of a very rugged, inhomogeneous, and very filamentary layer blanketing the photosphere.

Beginning at the chromosphere, the geometry of the individual structures is increasingly dominated by the local magnetic field. At the lower transition region ($T \leq 2 \times 10^5$ K), the structures strongly reflect the morphology of the underlying supergranular network. As the magnetic pressure overtakes the gas pressure leading to the low beta corona, the percentage of emission in filamentary loops steadily increases until the network completely disappears at temperatures above $10^6$ K. It may seem that a straightforward interplay between heating and morphology takes place in the transition region, but this is not the case.

The traditional picture of the transition region as the interface between the footpoints of large-scale structures and their coronal tops was contradicted by the weakness of its observed emission (Landi and Feldman, 2004). While the emission in the upper TR ($T > 2 \times 10^5$ K) can be understood in terms of heat conduction from the corona along magnetic field lines, the lower TR ($T < 2 \times 10^5$ K) cannot. Instead, this plasma forms a completely separate component of the solar atmosphere (Feldman, 1983, 1987). This component can consist of small cool loops (Antiochos and Noci, 1986; Dowdy, Rabin, and Moore, 1986; Feldman, Dammasch, and Wilhelm, 2000; Peter, 2001) that are best seen in the Quiet Sun and that probably correspond to the upper reaches of the mixed polarity magnetic carpet (Schrijver *et al.*, 1997). Feldman, Dammasch, and Landi (2009) showed that the differential emission measure (DEM) of the TR has the same shape everywhere (coronal holes, Quiet Sun, active regions) while coronal DEM of the very same regions are very different. Why and how are transition region loops different from higher arching coronal loops? Are they also comprised of unresolved strands? Are they heated in a fundamentally different way? Recently, Judge (2008) proposed a radically different view of the transition region emission, suggesting that it may result from cross-field diffusion of plasma from very fine cool threads extending into the corona (*e.g.*, spicules) and its subsequent ionization. Cool threads gradually expand in thickness as the ionizing front expands across the field lines and emits at TR temperatures, and provide images of the transition region similar to those observed by the Solar Ultraviolet Measurements of Emitted Radiation (SUMER) (Wilhelm *et al.*, 1995) spectrometer aboard the Solar and Heliospheric Observatory (SOHO).

*Hinode* observations revealed a dramatically new picture of the solar chromosphere and demonstrated its potential importance for the dynamics, energy, and mass supply of the transition region and corona. High temporal ($\simeq 5$ s) and spatial ($\simeq 0.2''$) *Hinode*/Solar Optical Telescope (SOT) observations showed that the chromosphere is much more structured and dynamic than previously believed. SOT revealed a chromosphere hosting a wealth of wave and oscillatory phenomena manifested as longitudinal and transverse motions within structures at the resolution limit (de Pontieu *et al.*, 2007b; Ofman and Wang, 2008; Okamoto *et al.*, 2007). Even a fraction of the inferred wave energy flux can account for the

coronal energy losses if it reaches the corona. SOT also showed that a significant fraction of observed spicules ("Type II"), known for decades to dominate the chromospheric landscape, disappear very rapidly (de Pontieu *et al.*, 2007b). This was interpreted as a signature of the plasma heating up to transition region and coronal temperatures; the mass contained in these disappearing spicules is sufficient to account for the mass present in the corona.

Capturing the fine spatial scales and rapid temporal evolution of the chromosphere and transition region plasmas represents a considerable observational and technical challenge. Nonetheless, recent significant improvements on instrumentation and image processing achieved both from ground (*e.g.*, Puschmann and Sailer, 2006; Rutten, van Veelen, and Sütterlin, 2008; de Pontieu *et al.*, 2007a) and spaceborne instruments (*e.g.*, de Pontieu *et al.*, 2007b), reaching, in all cases, spatial resolution under 1″ for plasmas at chromospheric regimes. Reaching these resolutions on the TR involves the use of strong ultraviolet (UV) lines, accessible only above Earth's atmosphere.

The Very high Angular resolution ULtraviolet Telescope (VAULT; Korendyke *et al.*, 2001), a sounding rocket payload, is the only instrument that has observed this critically important layer of the solar atmosphere at such high resolution. VAULT is specifically designed to obtain high spectral purity, zero dispersion spectroheliograms in the Lyman-α (1216 Å) resonance line of hydrogen. This emission line emanates from plasmas at 8000 to 30 000 K (Gouttebroze, Vial, and Tsiropoula, 1986). The Ly α radiation directly maps the dominant energy loss from plasmas at these temperatures, which correspond to the lower TR (Fontenla, Reichmann, and Tandberg-Hanssen, 1988). This instrument is the latest in a long and distinguished line of solar optical instruments obtaining observations in the Ly α emission line (Purcell and Widing, 1972; Prinz, 1974; Bartoe and Brueckner, 1975; Bonnet *et al.*, 1980). The VAULT observations are the highest quality UV observations of the solar atmosphere ever obtained and are a considerable improvement over previous instruments. Each rocket flight obtained observations with observable structures of $< 0.5''$ spatial scale, exposure times of 1 sec with a 17 sec cadence, and a $355'' \times 235''$ instantaneous field-of-view (FoV).

The VAULT data, and more recently, the *Hinode*/SOT observations invigorated the debate about the nature of the solar transition region. Not surprisingly, Ly α telescopes are planned for the upcoming *Solar Orbiter* mission and possibly the proposed *Solar-C* mission. It is, therefore, an appropriate time for a review of the VAULT observations. We believe that, as a trailblazer project in the exploration of the upper chromosphere-corona interface, the VAULT experiences will be a useful reference for the instrument design and science operations for those missions. We also take this opportunity to present the final calibration of the data and introduce the project website where all the data are publicly available. This article presents a detailed examination of the Ly α structures near the base of the solar corona obtained during the second flight of the payload (hereafter, VAULT-II). We are specifically concerned with those plasmas whose temperatures lie between 8000 and 30 000 K, ranging roughly from ∼2000 km to ∼60 000 km above the photosphere.

The article is organized as follows. Section 2 describes the latest instrument calibration and the observations from the second VAULT flight. Section 3 summarizes the importance of the Ly α in the frame of coronal and TR models. Section 4 discusses the sources of Ly α emission as determined in the VAULT images. Sections 5, 6, and 7 focus on, respectively, prominences, Quiet Sun, and spicules. We discuss our findings and conclusions in Sections 8 and 9.

## 2. Data Analysis and Observations

VAULT was successfully launched twice (7 May 1999 and 14 June 2002). Using the experience from the first flight (Korendyke *et al.*, 2001), the instrument performance during the second flight was improved by using a higher transmission Ly $\alpha$ filter (higher throughput) and better filtering of the power converter output (lower noise/higher quality data). So we concentrate on the VAULT-II images for the remainder of the article.

VAULT-II was flown on 14 June 2002 from White Sands Missile Range onboard a Black Brant sounding rocket. The observations took place around the apogee of the parabolic trajectory while the rocket was above 100 km. This minimum altitude was chosen to minimize absorption effects from the geocorona (Prinz and Brueckner, 1977). The duration of science operations was 363 sec and the rocket peaked at an altitude of 182 miles (294 km). The entire flight, from launch to recovery, lasted 15 min.

### 2.1. VAULT-II Observations

VAULT-II obtained 21 images from 18:12:01 to 18:17:47 UT with a cadence of 17 sec. The integration time was 1 sec for all frames except for a 5-sec image (the second in the series, not shown here). The target was an old active region complex near the East limb that included National Oceanic and Atmospheric Administration (NOAA) regions 9997-9999, Quiet Sun, filaments, plage, and the limb.

Figure 1 is a composite image of all VAULT-II frames. The composite FoV covers nearly 10% of the total visible solar disk area. To investigate possible center-to-limb variation (Miller, Mercure, and Rense, 1956) we calculate the radial median intensity of non-active region area (excluding plage region, prominences, and flaring regions). We do not find any significant center-to-limb gradient in agreement with Curdt *et al.* (2008).

The VAULT flight was supported by several other instruments. All corresponding data (see Table 1) are available on-line or per request. All VAULT data are publicly available on-line in Flexible Image Transport System (FITS) format and compatible with SolarSoft mapping routines. The images are interaligned, the dark level is subtracted, and an *ad hoc* synthetic flat-field is also created and provided with the data, but not applied on the on-line set. The flat-field is generated by retrieving the median (in time) pixel value as the solar image moves during the observations. It, therefore, accounts for flat-field and scattered light. Intensities are left in digital units (DN).

To improve the visibility of faint, small-scale structures, we apply a wavelet enhancement technique (Stenborg, Vourlidas, and Howard, 2008). This method decomposes the image into frequency components (scales). The frequency decomposition is achieved by means of the so-called *à trous* algorithm. With this method we can then obtain an edge-enhanced version of the original image by assigning different weights to the different scales upon reconstruction. We note that the aforementioned decomposition does not create orthogonal components, and therefore, the reconstruction does not conserve the flux. It is also possible to retain the low-scale information by adding a model background image. Both processed data, with and without the model, are freely available in the VAULT website. The level 0.9 VAULT-II data, together with the IDL-SolarSoft routines, composite full field image, flat-field, and wavelets processed data are available under: http://wwwsolar.nrl.navy.mil/rockets/vault/.

### 2.2. Spatial Resolution

The rocket pointing accuracy is $\sim 1$ arcmin with exceptional pointing stability of $0.25''$ peak-to-peak over 10 sec. To obtain the solar coordinates, rotation relative to Solar North,

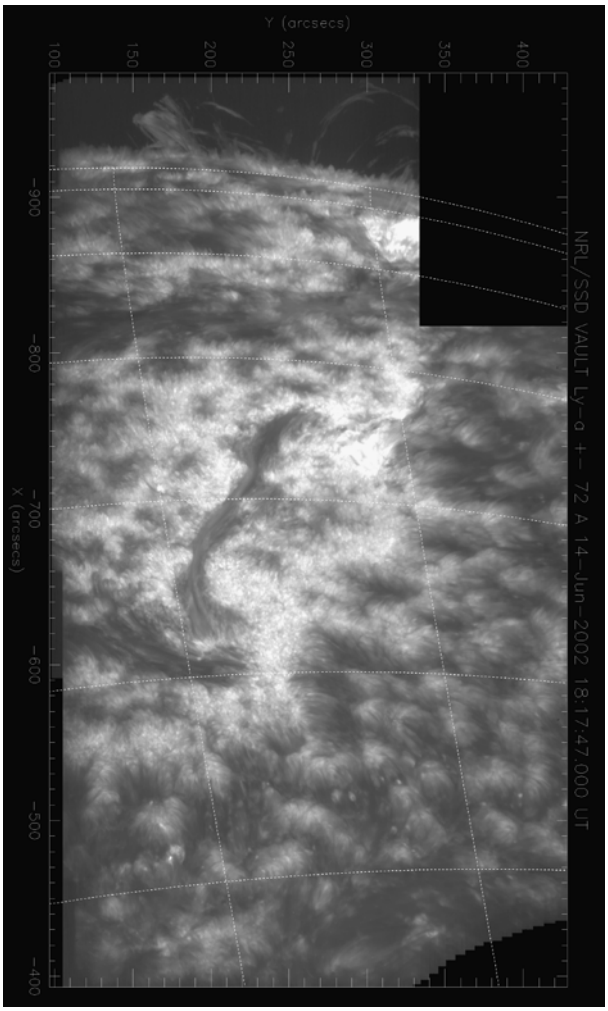


**Figure 1** The total solar field-of-view observed during the second VAULT flight. The image is a composite of all VAULT-II observations after dark current subtraction and flat-fielding. It covers a $\sim 600 \times 450$ arcsecs area, with $0.12''$ pixel size. Solar North is to the right and Solar East at the top of the image. The image is plotted with histogram equalization of the intensities.

**Table 1** Joint observing campaign supporting the VAULT-II launch.

| Telescope | Channel | Cotemporal time series |
|---|---|---|
| SOHO | MDI/EIT/CDS | EIT-304 Å partial FoV |
| TRACE | 171, WL, 1600 | 171 Å, partial FoV |
| BBSO | Hα, Ca, $B_{LOS}$, WL | Hα, partial FoV |
| Kitt Peak | Mgram | Photospheric magnetogram |

and pixel size for the VAULT-II images we use *Transition Region and Coronal Explorer* (TRACE) Ly α images taken only minutes apart from the VAULT images. Figure 2 shows the alignment results. The resulting VAULT pixel size is $0.125'' \times 0.110''$, which is in excellent agreement with the optical design expectations (Korendyke *et al.*, 2001). During the flight, a small thermal expansion of the spectrograph structure relative to the primary mirror resulted in an apparent pointing drift that was variable, but less than $\approx 3$ pixels $\sec^{-1}$. If

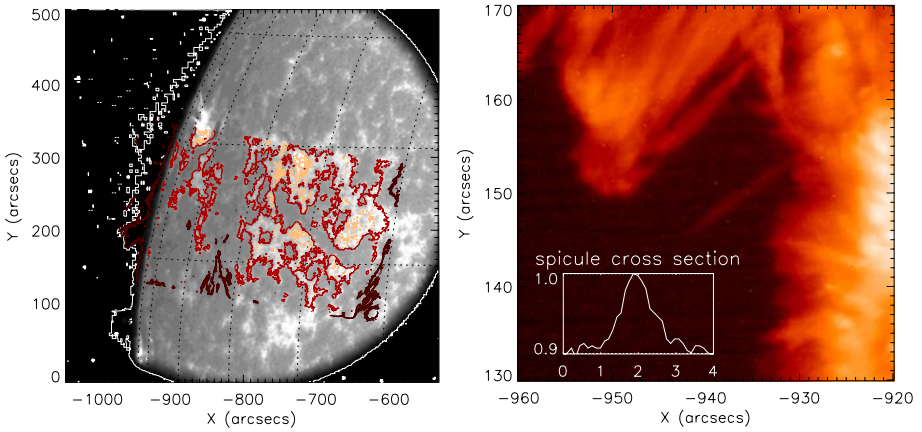


**Figure 2** Left: Alignment of VAULT-TRACE Ly α images. We find the best correlation by optimizing the position, rotation, and scale in both $x - y$ directions. We derive a pixel size of $0.125'' \times 0.110''$. The TRACE Ly α was taken at 18:18:54 UT (black-and-white figure and white contour), the VAULT was taken at 18:17:30 UT (three red contours). Right: Estimation of the VAULT resolution using the thin spicule located at the center of the image. The median normalized cross section (in arcseconds) of the spicule along its length (plot inset in figure) is fitted with a Gaussian, which leads to a FWHM $\approx 0.49''$ as an upper limit.

it was uniform during the flight, this drift will place a conservative lower limit on the instrument resolution of $\sim 0.75''$ ($0.375''$ pixel$^{-1}$). However, we can visually identify smaller structures (always in absorption on the disk) in several images. To better estimate the actual image resolution, we measure the full width at half maximum (FWHM) of the smallest structure we can find in the images. We use the median cross section along the 110-pixel length of the thinnest spicule, located at the center of Figure 2 (right), and fitted it with a Gaussian. The FWHM $\approx 2.35 \cdot \sigma$, where $\sigma$ is the standard deviation of the fitted Gaussian profile. This leads to a VAULT-II resolution of $0.49''$. However, the upper limit may be dictated by opacity effects rather than instrumental ones.

The photometric calibration of the instrument was originally determined from the observations during its first flight in May 1999. The calibration factor from DN's to intensity (ergs s$^{-1}$ cm$^2$ sr$^{-1}$) is deduced by comparing the average emission (in DN's) of an area of the Quiet Sun to the Quiet Sun intensity obtained by Prinz (1974). This is a reasonable assumption since both observations were made at similar phases of the cycle; the majority of the VAULT-I field-of-view contained Quiet Sun and the Prinz (1974) measurements were well calibrated ($\sim 20\%$).

A comparison to the SUMER spectrograph Ly α observations is made to improve on the radiometric accuracy of our measurements. The first issue is the spectral purity of the signal. The VAULT gratings transmit solar light in the range of 1140 – 1290 Å. In this range there are only a few relatively bright lines, the brightest of which is Si III at 1206.51 Å. SUMER Quiet Sun spectra show that almost all ($\sim 95\%$) of the emission in this range comes from the Ly α (assuming a rectangular filter). Concerning the spectral purity on the full range above 120 nm, our calculations show that the signal should be 70% pure.

Since the SUMER instrument has a photon counting detector with no dark signal, there is no background to be removed from the SUMER data. To establish the comparison with SUMER we assume that the normalized radiance frequency distributions over Quiet Sun areas produced with data from the two instruments should be equal or very similar to each other. To account for the different spatial resolution we also compute the radiance frequency

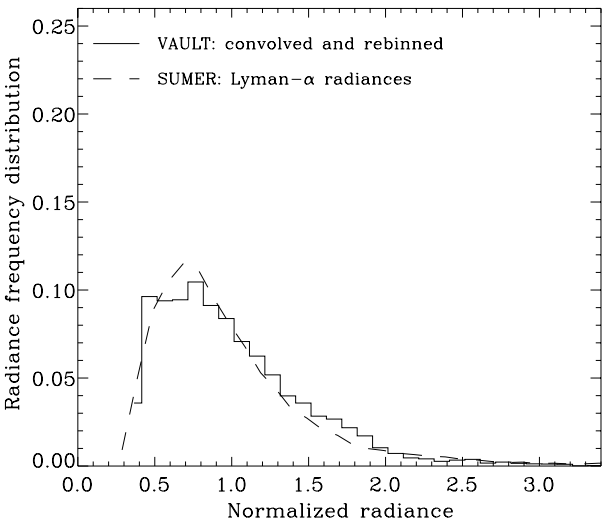


**Figure 3** Normalized H I Ly α distributions as obtained from the SUMER data (dashed line) and the VAULT data (solid line) rebinned and convolved to match the SUMER spatial resolution after subtracting a background signal level of 80 DN $s^{-1}$ (see Section 2.2).

distributions after convolving the VAULT data with a two-dimensional Gaussian function (of 12 pixel = 1.5″ FWHM, equal to the SUMER spatial resolution) and binning over 8 × 8 pixels to yield the SUMER pixel size of ≈ 1″. The comparison reveals that a low-level signal of about ∼ 80 DN $s^{-1}$ needs to be removed from the VAULT images to bring them in accordance with the SUMER measurements (Figure 3). After a careful examination of the VAULT-II images, we find a noise pattern of 83 ± 20 DN $s^{-1}$, which is variable from image to image and cannot, therefore, be removed with the dark current subtraction. We trace the source of the noise to interference from a faulty ground when the payload is switched to battery power.

The final step is a comparison of the Quiet Sun level in our images with an average Quiet Sun radiance measured at Earth as we did for the first flight. For the VAULT Quiet Sun level we use the peak of the histogram of the image intensities (in DN $s^{-1}$) minus the 83 DN's of the background signal. The Quiet Sun level was 217 ± 20 DN $s^{-1}$. The SUMER average Ly α radiance on the Quiet Sun in 2008 was 73 ± 16 W $m^{-2}$ $sr^{-1}$. This is well within uncertainties with the Prinz (1974) measurement of 78 ± 16 W $m^{-2}$ $sr^{-1}$. We adopt the latter value for consistency with our VAULT-I results and because it was obtained about two years after maximum and may better compare with our 2002 data. In this case, we derive a calibration factor of 1 DN $s^{-1}$ = 0.359 ± 0.081 W $m^2$ $sr^{-1}$.

## 3. The Interpretation of the Ly α Emission

The hydrogen Lyman-α line, the strongest line of the solar spectrum, is a $1s\,^2S_{1/2} - 2p\,^2P_{1/2,3/2}$ doublet resonant line at 1215.67 Å. The FWHM of the line core is very broad (∼ 1 Å) due to Stark and Doppler broadening and the high optical thickness. The line center probably forms in the lower TR (∼ 40 000 K; Vernazza, Avrett, and Loeser, 1981) while the wings form in the chromosphere (∼ 6000 K) by partial redistribution of the core emission. Thus, the Ly α line plays a critical role in the radiation transport in the chromosphere/TR interface. Below 8000 K, model calculations show that the line is very close to detailed balance. For temperatures between approximately 8000 and 30 000 K, the dominant energy loss is through Ly α emission. For temperatures higher than about 30 000 K, Ly α

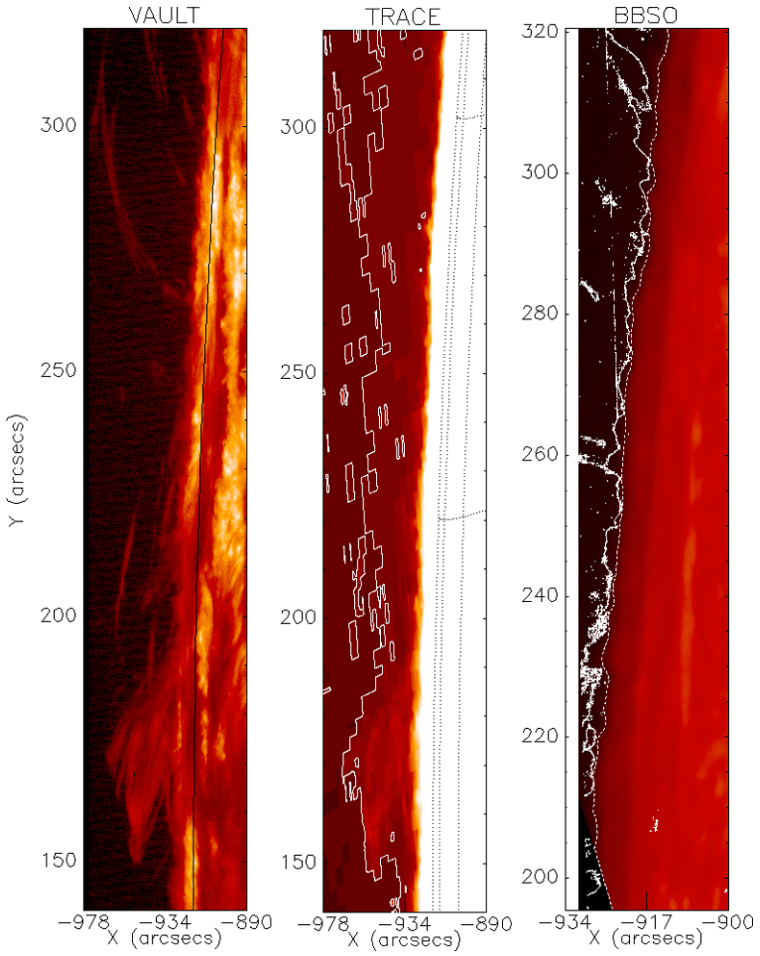


**Figure 4** VAULT-II, TRACE Ly α, and BBSO Hα comparison of the solar limb. All intensities are individually trimmed and scaled to emphasize the fainter details. Left: VAULT-II (18:17:13 UT) after alignment and calibration. The black contour follows the visible limb, as aligned with the TRACE white-light channel. Center: TRACE (18:18:54 UT) Ly α. The black grid denotes the photosphere. The prominence is much fainter than in the VAULT images, but it is still visible. The white contour close to noise level helps to correlate with VAULT. Right: Hα channel (19:16:41 UT) from ground-based BBSO. The BBSO FoV is slightly smaller than that of the other instruments. The dotted contour denotes the VAULT edge. Note that the Hα spicule heights are up to $\sim 2''$ shorter than in Ly α.

is transparent (Gouttebroze, 2004). The physics of this line were explored in a number of articles (Vernazza, Avrett, and Loeser, 1981; Gouttebroze, Vial, and Tsiropoula, 1986; Woods *et al.*, 1995; Fontenla, Avrett, and Loeser, 2002; Gouttebroze, 2004) and the average full-Sun line profile and its variation over the solar cycle was measured by the SUMER instrument (Lemaire *et al.*, 2004), but most deal with the spectral characteristics and are of more interest to spectroscopic analysis. On the contrary, VAULT data consist of the integrated line intensity over a wide bandpass, which includes contributions from other lines such as Si III, N I, N V, and C III. Because of the complexity of the line, model calculations are the easiest way to interpret imaging observations. Past analysis was based on plane parallel radiative transfer models using the Ly α contrast (the ratio of the Ly α

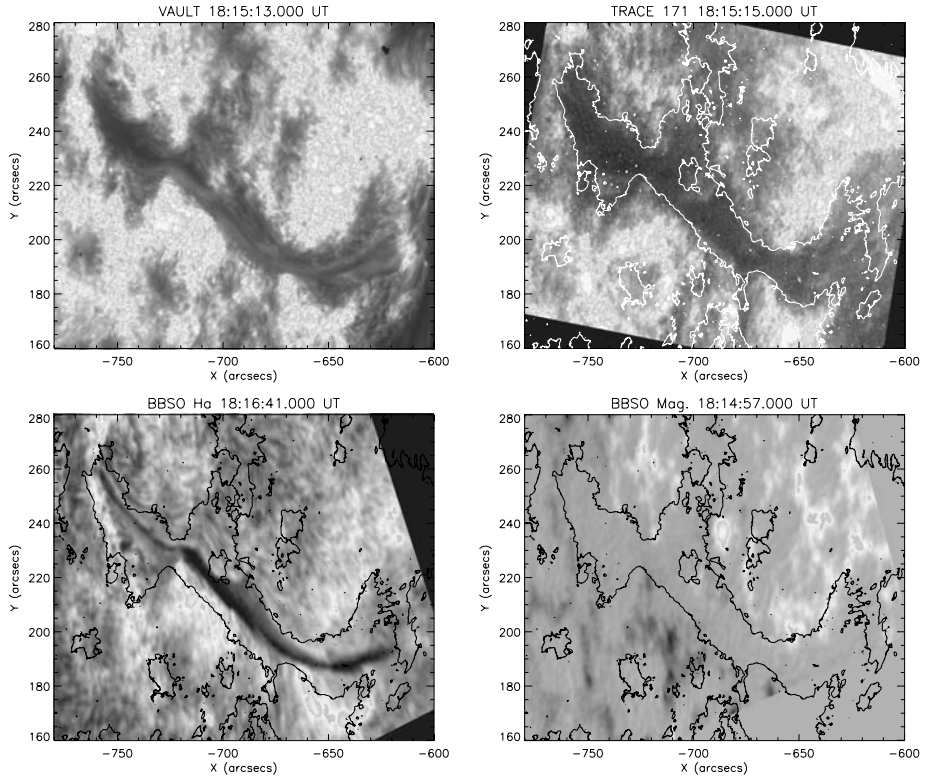


**Figure 5** Prominence as seen in almost simultaneous observations with various instruments. The contours mark the outer envelope of the Ly α prominence. The field-of-view is the same. Top left: VAULT Ly α. Top right: TRACE 171 Å. Bottom right: BBSO photospheric magnetogram. Bottom left: BBSO Hα center.

emission of a structure relative to the average Quiet Sun) to derive estimates of pressure and temperature within the observed structures (Bonnet and Tsiropoula, 1982; Tsiropoula *et al.*, 1986). Recent computational and theoretical improvements enabled the calculation of the emission from models with more realistic cylindrical geometries (Gouttebroze, 2004), and therefore, direct comparison with observed Ly α intensities (Gunár *et al.*, 2006; Patsourakos, Gouttebroze, and Vourlidas, 2007). However, calculations from the latter models remain time consuming and difficult to apply over the wide range of structures seen in the VAULT images. Since the scope of our article is to present a broad overview of the Ly α atmosphere, we return to the plane parallel assumption and adopt the approach of Tsiropoula *et al.* (1986) to estimate physical parameters for the structures in our images. More careful analyses of specific features will be undertaken in the future.

The calculations in Gouttebroze, Vial, and Tsiropoula (1986) required the calculation of the ratio of the intensity of a given structure over the average intensity over the solar disk or "Ly α relative intensity" (LRI). Since we do not have full disk images in Ly α we cannot directly compute a solar disk average. However, the disk emission is dominated by the Quiet Sun (Figure 5 in Prinz, 1974) and we, therefore, need only to calculate the Quiet Sun level. Thanks to the large FoV, the VAULT images contain large Quiet Sun areas. So, we use the median of the lower part of the FoV $\sim (x \in [-550, -400], \forall y)$ in Figure 1 as the "Quiet Sun" level. We then calculate the LRI range for several representative features.

**Table 2** Qualitative plasma diagnostics for several types of structures. See Section 3.

| Structure | Intensity [LRI][a] | Radiance [$10^{12}$ ergs cm$^{-2}$ s$^{-1}$ sr$^{-1}$] | Opt. Depth Log | $T$ [$10^3$ K] | Pressure [dyn cm$^{-2}$] |
|---|---|---|---|---|---|
| Quiet Sun | 0.5 – 5 | 3.3 – 32.5 | 4 – 5 | 8 – 10 | 0.1 – 1 |
| Quiet Sun Prom. | 0.2 – 1.4 | 1.8 – 9.5 | 6 – 3 | 7 – 9 (20)[b] | 1 (0.1)[b] |
| Plage | 5.7 – 12 | 37.5 – 75.0 | 4 | 10 – 13 | 1 |
| Plage Prom. | 1 – 5 | 6.7 – 32.5 | 3 – 0 | 8 – 40 | 0.1 – 1 |
| Off-limb Prom. | 0.8 – 1.1 | 5.8 – 7.8 | 3 – 0 | 15 – 80 | 0.1 – 1 |
| Off-limb Loops | 0.4 – 0.5 | 2.8 – 3.8 | 0 | 30 – 40 | 0.1 |

[a]Ly α relative intensity (LRI). LRI = 1 represents median of Quiet Sun region.

[b]Likely to have reduced optical thickness. High values reflect underlying plage.

The results are shown in Table 2. The corresponding pressure, temperature, and optical thicknesses derived from Gouttebroze, Vial, and Tsiropoula (1986) are also included. The numbers suggest that most solar structures are optically thick in Ly α even at temperatures departing significantly from chromospheric ones ($\geq 10^4$ K). Quiet Sun emission seems to arise at the chromosphere while plage, prominence, and off-limb structures have lower TR temperatures and are presumably located at larger heights. These results are in agreement with the earlier measurements of Tsiropoula *et al.* (1986) except for the minimum LRI values. Tsiropoula *et al.* (1986) reported values as low as 0.05, but did not observe LRI below about 0.2 anywhere but at the edges of off-limb loops. The difference is most likely due to higher sensitivity and spectra purity of the VAULT instrument, which should increase the detected counts of the fainter structures and minimize the continuum contribution to the Quiet Sun levels relative to past instruments. The faintest structures (LRI $\sim 0.2$) seen in the VAULT images are long, thin strands seen in absorption against the network. These strands are also the smallest resolved structures with the lowest temperatures (Table 2). They are very similar to chromospheric filaments, but they do not seem to be associated with any large-scale structure. Their origin is currently a mystery, but they can be cooling loops. The best candidates for optically thin emission are the off-limb loops seen in the northeastern edge of the VAULT FoV. The observed LRI range of 0.4 – 0.5 can be consistent with either chromospheric ($< 10^4$ K) or TR emission. These loops were not detected in the Big Bear Solar Observatory (BBSO) Hα images, and thus we select the higher temperature solutions ($T \sim 3 – 4 \times 10^4$ K) for them.

Table 2 serves as a concise description of the physical parameters of Ly α structures and we will refer to it in our subsequent discussions of individual features, starting with the contribution of each of these features to the overall Ly α intensity.

## 4. Sources of the Ly α Intensity

Ly α is a very optically thick line and results in both emission and absorption depending on the properties of the surrounding plasma. This interplay is at the region where the plasma starts to be dominated by the magnetic fields, creating a wide range of intensities. In addition, the strength and variability of the Ly α irradiance has important effects on Earth because it affects the chemistry of the mesosphere (*e.g.*, ozone layer) as well as the climate on longer time scales. Only the central part of the broad spectral profile of the solar Ly α

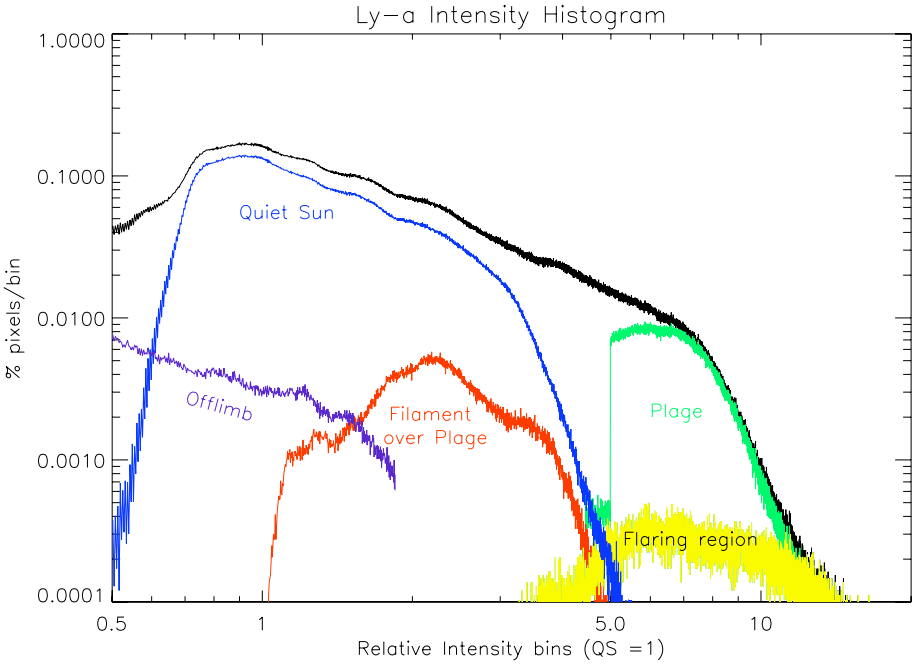


**Figure 6** Ly α emission histogram (black line). Different colors represent partial histograms from the labeled subregions. In particular we note that the "Quiet Sun" emissions span one order of magnitude. Intensities are scaled to the median Quiet Sun level. Plot ordinates scaled to total number of data pixels. Cover area for each type (integral over the histogram curve) is: Total (black line): 100%, Quiet Sun: 61%, Plage: 13%, Filament: 2%, Flaring region: 1%, Off-limb: 1%, Rest: 23%. See Section 8 for more details.

emission is effective for the geoenvironment, but there is a clear relationship between the central radiance of the solar Ly α line and the total irradiance of the line (Emerich *et al.*, 2005). To understand changes in Ly α irradiance we first need to identify the contributions of the various solar sources of this emission to the total Ly α irradiance.

We attempt a first cut at this problem using our spatially resolved, calibrated images. As we discussed earlier, we are able to differentiate among Quiet Sun, plage, prominence over plage, off-limb, and flaring regions. Figure 6 shows the corresponding intensity histograms for each domain (color coded), relative to the overall histogram (black line). The values are constructed from the pixels inside each region, and considering the median value for each pixel in time (from Figure 1):

*Quiet Sun (blue line):* We select a region around the lower-right corner in Figure 1 as typical Quiet Sun. Based on this selection, the Quiet Sun covers 61% of the pixels. We use the median value of the Quiet Sun as a normalizing factor. Normalized values inside this region, however, span from 0.5 to 5. The Quiet Sun exhibits a wide range of intensities, as it can be expected by the high optical thickness and strong structuring of the plasma. The low end of the histogram reaches the edge detection of off-limb prominences, while the high end reaches the plage levels. Scattered around this Quiet Sun we find several cases of localized brightenings that may be related to explosive events, which we discuss in Section 6.

*Plage (green line):* The central part of the VAULT FoV shows a bright plage. Following a similar method as for the Quiet Sun, we find that the plage covers 13% of the pixels, without considering the central overlying filament. Typical normalized intensities range from 5 to 15.

The only other contribution at these levels comes from the flaring region at the North edge of the image. This means that one approximation to the total solar Ly α irradiance can be obtained using the Quiet Sun level adding a multiplying factor ∼ 7 for the percentage of the disk corresponding to plages (which can be obtained from other lines like Ca).

*Filaments over plage (red line):* Our results show that the plasmas in the filaments over the plage are sufficiently opaque to reduce the observed intensity to Quiet Sun values. This particular filament blocks the central 22% of the plage area.

*Off-limb (purple line):* The VAULT images contain several examples of limb structures, including spicules. As we discuss later, we find higher heights for the spicules compared to Hα. Large overlying loops reaching projected heights of 60″ can also be observed. The emission from these structures indeed shows Quiet Sun levels, down to our detection threshold for the histogram (0.5). It is likely that these structures are nearly optically thin, implying temperature $\gtrsim$ 30 000 K. The large heights imply a dynamic state for these loops and they are probably associated with catastrophic cooling episodes studied previously with TRACE (Schrijver, 2001).

## 5. Prominence and Filament Observations

The images contain a large number of filaments, filamentary structures, and a prominence. It is also the first time that the fine-scale structure of the filaments is resolved in this wavelength. Figure 7 reveals a highly organized filament comprised of parallel threads with little, if any, twist. No obvious twist is evident in any of the other filaments either. The threads have a typical width of around 0.5″ or less, and are seen as intensity enhancement profiles of about 5%. Figure 7 also shows a stable and detached thread with a width reaching the instrument resolution and 30% absorption over the underlying plage. The filament is further analyzed in Millard (personal communication) where the comparison with the Hα observations suggests that Ly α traces the cool outer plasma while Hα originates from the coolest part of the filament. There is also evidence for uneven absorption across the filament axis. The northern side shows evidence of Ly α absorption, while the southern side shows absorption only in the coronal lines (171 Å ) consistent with the presence of a void or cavity around the filament. The northern absorption can be understood as a line-of-sight effect from low-lying absorbing plasma at the filament flanks.

The last panel in Figure 4 shows the size discrepancy between Ly α and Hα observations. Only a small knot, ∼ 5″ width, of Hα emission is visible, whereas the Ly α prominence extends for almost 50″.

## 6. Quiet Sun Observations

The Quiet Sun was the testing ground for various theories and concepts of the structure of the solar atmosphere. It is not surprising then that it is also the area where VAULT observations generated the most interesting results (Patsourakos, Gouttebroze, and Vourlidas, 2007; Judge, 2008). Earlier observations showed that Ly α emission is concentrated along the supergranular lanes in clumps with small loop-like extentions toward the cell interiors. Faint emission without spatial structures is detected at the cell centers. VAULT images, especially VAULT-I which covered a much larger Quiet Sun area, resolved the spatial structure in the clumps along the supergranular boundaries (Figure 8). The Quiet Ly α Sun area shows groupings of filamentary plasma, similar to the Hα rosettes, with a typical diameter of

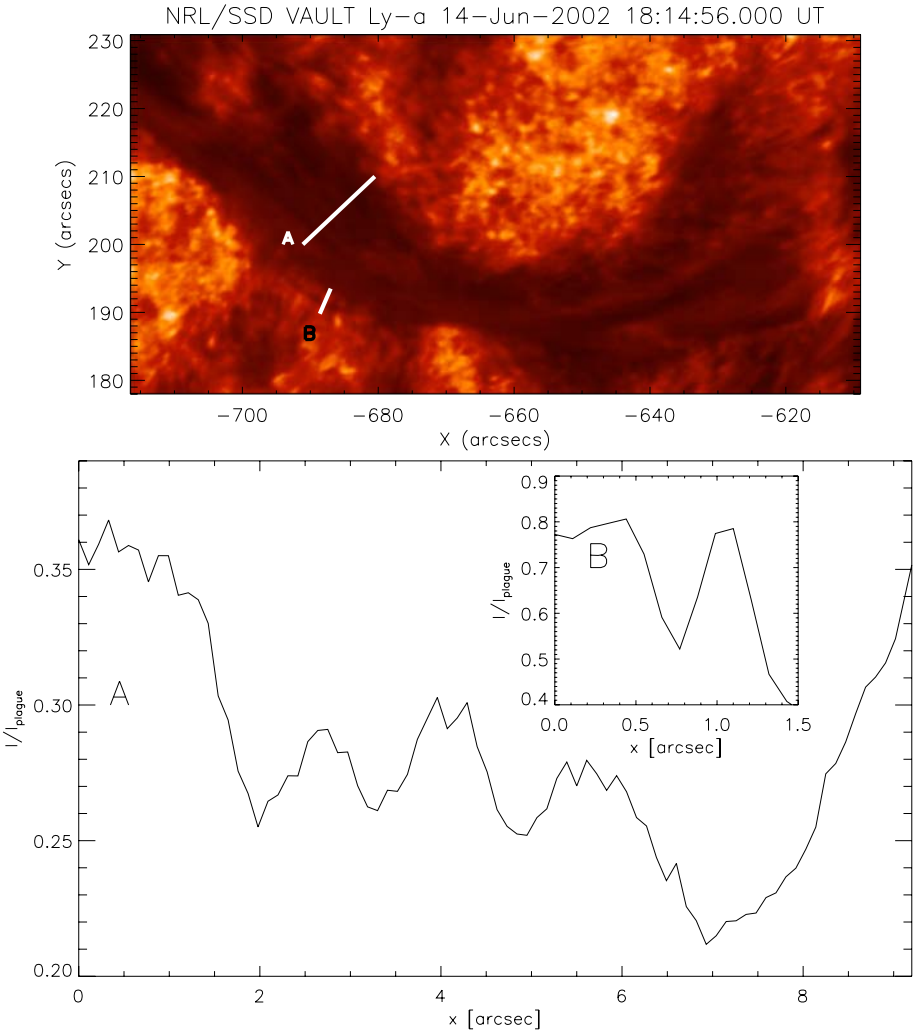


**Figure 7** Prominence shows reduced absorption threads along its axis below 0.5″. This supports a nonaxisymetric prominence. Top: Single VAULT frame, with labeled segments for the perpendicular cuts (labeled as "A" and "B"). Intensities are not scaled. Bottom: Intensity profile perpendicular to the prominence axis for "A" segment and "B" detached thread (plot inset). Intensities are scaled to surrounding median plage value.

∼23″. These rosettes show filamentary structure up to the resolution limit of the instrument, of about 0.4″. This grouping in rosettes is stable through the observations (∼6 min), but shows the presence of localized brightening events with a timescale variation 60 – 120 sec and sizes of a couple of arcseconds. The network structures rise above the chromosphere about 7100 km or 10″ as seen in Figure 4. This measured value is consistent with previously measured values of the height of the transition region above the limb. Their location at the supergranular cell boundary uniquely identifies these loops as being the byproduct of convective motion driving together magnetic fields at the edges of the supergranular cell.

The outer areas consist of short loop-like structures while the centers of the clumps have a more point-like nature. This morphology is consistent with loops of progressively higher

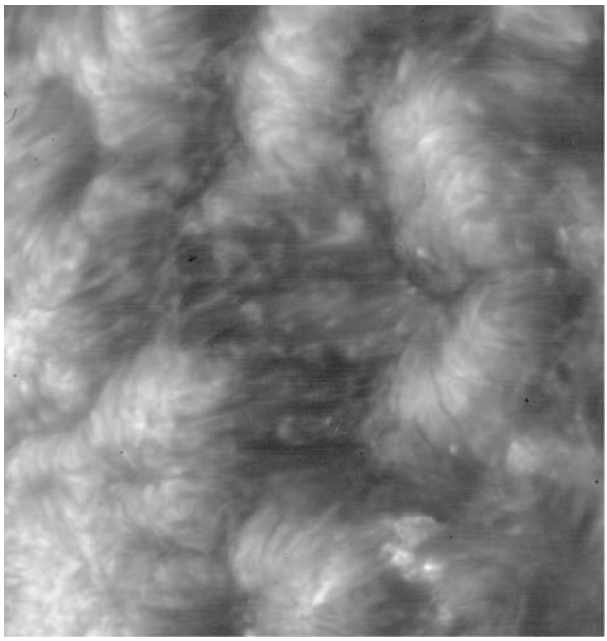

**Figure 8** Detail of a supergranular cell in the Quiet Sun in Ly α. The horizontal extent is 121″ and the vertical is 117″ and the field-of-view is centered at around (− 500″, 250″) in Figure 1. This is an example of the first spatially resolved images of the Ly α emission of a cell interior.

inclination toward the center of the boundary. The obvious question is whether the more extended Ly α loops are full loops or just the lower part of a larger structure, possibly extending to higher temperatures. Patsourakos, Gouttebroze, and Vourlidas (2007) applied an analysis method used for coronal loops to a detailed Ly α emission model and found that the short loops at the edges of the boundary channel were consistent with full Ly α loops, and therefore, can account for the "cool" loops predicted by models of the transition region (Dowdy, Rabin, and Moore, 1986). However, the magnetic footpoints of these loops cannot be identified in photospheric magnetograms due to the lower spatial resolution and reduced sensitivity of the Michelson Doppler Imager (MDI) data. Although these problems should not affect the larger loops, their footpoints remain ambiguous. To address these problems, Judge and Centeno (2008) decided to investigate the magnetic origin of the extended Ly α loops using magnetic field extrapolations. They found that the longer Ly α loops originate near the boundary center and are more likely the lower extensions of large scale loops that connect areas much more distant than the neighboring cells. The extrapolations show that the smaller loops at the edge of the network lanes are indeed small-scale loops supporting the interpretations of Patsourakos, Gouttebroze, and Vourlidas (2007).

### 6.1. Cell Interior

Another new observation from VAULT is the imaging of Ly α emission from the cell interiors for the first time. As can be seen in the example of Figure 8, the emission extends over the full interior area and is structured in various spatial scales. The emission is filamentary, optically thick with some apparent dependence on the local radiation field. The associated time series (movies available in the on-line VAULT archive) reveal significant evolution in these structures, like flows and jets. The material within the filamentary structures shows an overall motion toward the network boundary similar to the motions of emerging magnetic field elements in photospheric magnetograms and white-light images. As the magnetic

field of opposing direction accumulates in the boundary, it is expected that some cancelation is taking place. Indeed, there are a few cases where Ly α material appears to jet out from smaller emission clumps creating a bright point. These events are never seen in the cell center and can originate from magnetic reconnection closer to the photosphere. Some examples can be seen along the column at $-500''$ in Figure 1. The limited resolution of available magnetograms has not allowed us to locate the origins of these jets.

### 6.2. Mircoflaring in the Quiet Sun

Although the VAULT time series show continuous motions and brightness evolution throughout the full field-of-view, there are very few strong enhancements that can qualify as a flaring emission. The short duration of the flight may be a reason for this, but we were able to isolate only 2 to 3 events. Figure 9 shows an example from a Quiet Sun feature that gives rise to a plasma jet rising from the cell center. The brightening was detected by SOHO/Extreme ultraviolet Imaging Telescope (EIT), which classifies it as a regular bright point. The event lasts for $\sim 500$ sec.

Since we have calibrate images, we can estimate the thermal energy of the Ly α flaring under some assumptions. We adopt Equation (5) in Benz and Krucker (2002)

$$E_{\rm th} = 3k_{\rm B}T\sqrt{EMV}, \tag{1}$$

where the energy $E_{\rm th}$ corresponds to Ly α plasma at temperature $T$ and emission measure $EM$ integrated over volume $V$. We assume $T = 2 \times 10^4$ K, $V = {\rm d}A\,{\rm d}l$, ${\rm d}A = 21'' \times 21''$ area, and ${\rm d}l = 0.5''$ equal to the mean free path of a Ly α photon for optically thick emission. For the estimation of $EM$ we adopt the calculations in Vourlidas *et al.* (2001) but use the updated photometric calibration reported here. The new $EM$ calibration for VAULT is $1\ {\rm DN\,s^{-1}\,pix^{-1}} = 3.74 \times 10^{26}\ {\rm cm^{-5}}$. To account for integrating the energies over an area that may contain both flaring and background (likely optically thin) emission, we subtract the emission from the first pre-event image from the plots. The resulting energy levels are very similar to those for coronal bright points (Krucker and Benz, 1998) as the EIT observation of plasma at $T \geq 8 \times 10^4$ K suggests. Unfortunately, we cannot tell whether there is any coronal emission from this bright point because it lies outside the TRACE field-of-view and EIT was observing solely in He I during the VAULT flight. We only report counts for the EIT light curves because there is only one wavelength available and the emission measure cannot be calculated (right axis in Figure 9). The VAULT and EIT curves are aligned at the pre-event emission level along the intensity axis to allow a comparison. The main conclusions from Figure 9 are that the Ly α and He II have a similar impulsive phase and the He II emission seems to be the extension of the cooler Ly α emission. This is also in agreement with the earlier results showing a delay from cooler to hotter coronal lines and extends the detection of heating events to a much lower layer of the atmosphere. The energy estimates in Figure 9 are in the range of microflares, which seems reasonable for the lower TR. An inspection of the plage area around the filament shows fainter brightenings that can still be classified as impulsive based on their light curves. Energy estimates for those brightenings are around $< 5 \times 10^{23}$ ergs, lower than a microflare. Figure 10 shows an example of such a brightening. The energy was estimated over an area of $\sim 1.8'' \times 1.8''$; all other assumptions are the same as above. Because these brightness changes are very close to the overall brightness variability of the plage, it is difficult to say with certainty that these are flaring events. A more sophisticated analysis is required, but it is beyond the scope of the article.

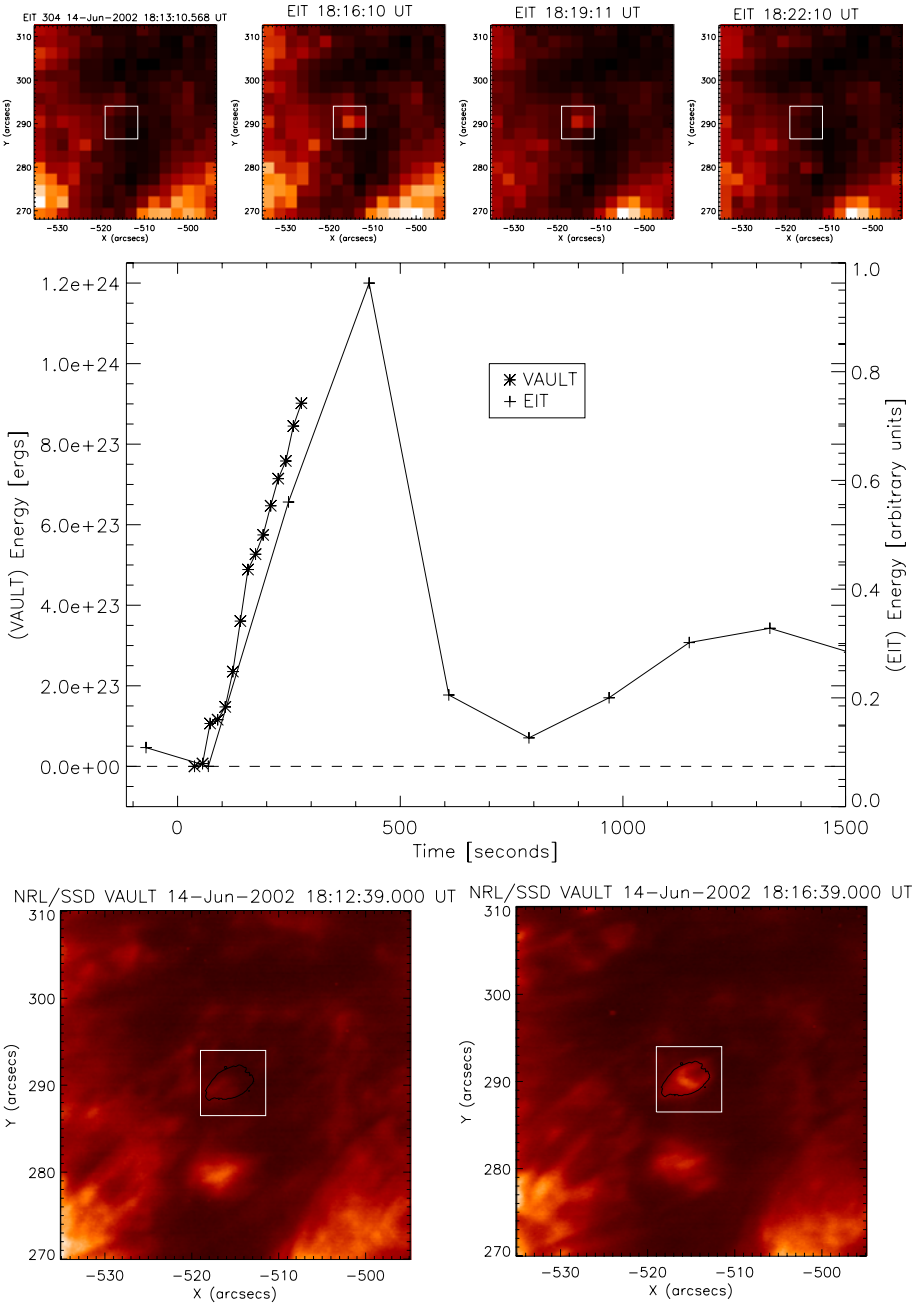


**Figure 9** Microflaring event in the Quiet Sun detected in Ly α and He II. Top panels: EIT He II images of the event (18:13, 18:16, 18:19, 18:22 UT, $40'' \times 40''$ FoV). Middle panel: Comparison of the energy curves from VAULT to the EIT light curve. The total counts within the black outline (VAULT) and within the white boxes (EIT) were used to calculate the curves. Bottom panels: Ly α images of the event at its initiation (left) and peak (right).

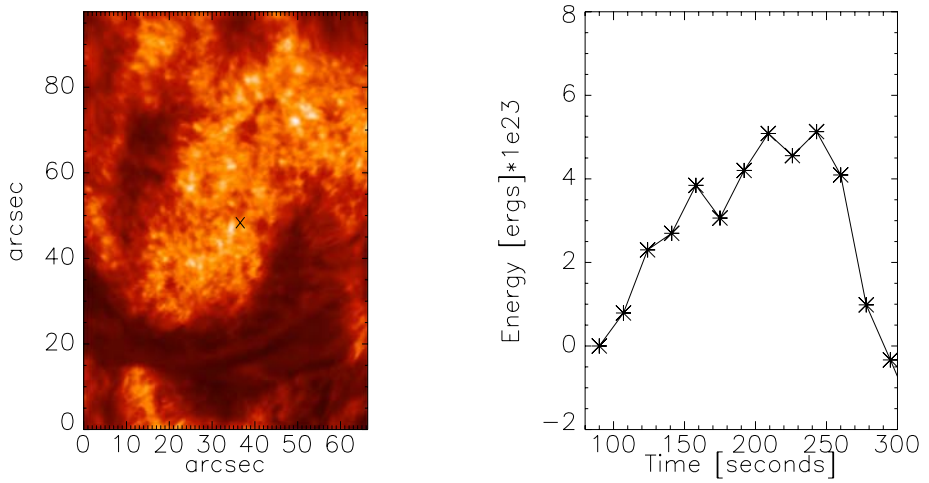


**Figure 10** Microflaring event in the Ly α plage. Left: The symbol "x"marks the location of the brightening. Right: The energy estimate for this event.

## 7. Plage and Spicules in Ly α

The active plage was studied in some detail using the first VAULT observations (Vourlidas *et al.*, 2001). The large degree of spatial structuring and the variability of these structures, combined with the complex radiative character of Ly α emission, complicate the detailed analysis of the plage. The plage has a clearly different morphology than the Quiet Sun. It lacks extended loop-like structures, but contains many point-like brightenings reminiscent of the 171 Å moss. Actually the TRACE 171 Å images show moss over the majority of the plage with large-scale loops located only in the periphery (Figure 5). As expected, the moss underlies hotter loops seen in the EIT Fe XV 284 Å images, but the Ly α brightness is not correlated with the degree of coronal heating above. A quick inspection of the Ly α and 171 Å images in Figure 5 shows that, despite the largely similar mossy appearance, there are several areas without a detailed correlation between corona and lower TR as noted before [*e.g.*, region R2 in Figure 2 of Vourlidas *et al.* (2001)]. Neutral hydrogen diffusion across field lines, as proposed by Judge (2008), may be an explanation of the uniform brightness of the plage in Ly α, but better calculations are needed before we can establish the viability of this mechanism.

### 7.1. Detection of Proper Motions

A significant part of the variability seems quite random. For a given pixel, the brightness change can be due to the weakening of the emission, the lateral motion of the bright point, or the appearance of dark (likely absorbing) features. We believe that these changes can be understood as the buffeting of the Ly α moss by chromospheric Hα jets, similar to the picture proposed by de Pontieu *et al.* (1999) for the 171 Å moss, but extending it to much smaller spatial scales.

Furthermore, we can identify coherent motions in several places. The most obvious ones can be found at or near the filament footpoints and along their backbone structure. Blobs of weakly emitting Ly α seem to flow toward the lower atmosphere. At the same time, apparently upward-moving blobs can also be seen at the filament footpoints, as well as along the

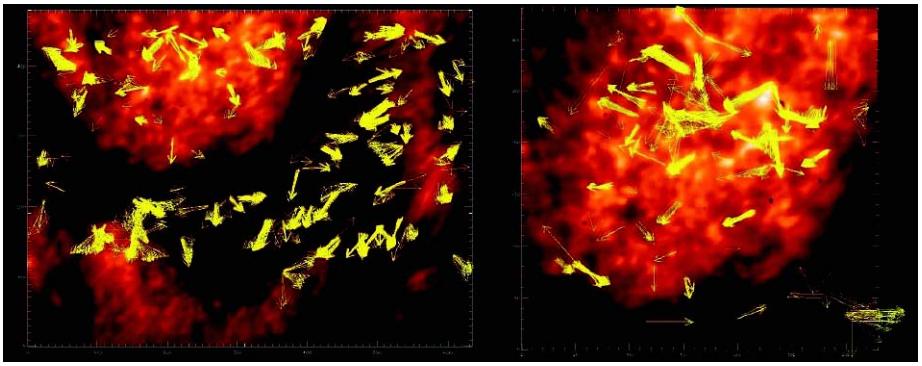

**Figure 11** Detection of proper motions in Ly α plage. The lengths of the displacement vectors are proportional to the estimated speed. Only pixels with correlation coefficients $\geq 0.3$ and intensity changes $\geq 3\sigma$ above the background are considered. The units are VAULT pixels ($0.112''$ pixel). Left: Filament and nearby plage. Upward motions can be seen along the western footpoint. Right: Plage detail. Note the counterstreaming motions along the filament boundary and diverging (explosive?) motions at certain bright points.

boundaries of the small network cell within the plage, and basically in most locations where there is high contrast with the background.

In an attempt to quantify these motions we use a local correlation method to track the blobs in time. To suppress the influence of the background buffeting motions we calculate the standard deviation, $\sigma$, of the intensity variability for each pixel at the peak of the emission and then consider only pixels with $\geq 3\sigma$ as inputs to the cross-correlation algorithm. The large degree of variability and spatial structuring results in many correlations. So we keep only the pixels with correlation coefficients higher than 0.3 and estimate their speeds and velocity vectors. We derive speeds in the range of $5-20$ km s$^{-1}$, which are similar to the speeds of chromospheric fibrils and spicules (*e.g.*, Wilhelm, 2000; Langangen *et al.*, 2008). In general, the cross-correlation results show motions in all directions, reinforcing the visual impressions of the large degree of randomness in the Ly α structures. However, a closer inspection of the displacement vector reveals several instances of coherent motions. In the example of Figure 11, we can see upward motions along the western filament footpoints and the filament boundaries. There is clear evidence of counterstreaming motions along the filament. Some of those are in the upper range of our estimated speeds ($\sim 20$ km s$^{-1}$) and are very close to Hα measurements in filaments (Engvold, 1998; Lin, Engvold, and Wiik, 2003). The nearby plage shows motions that follow the curvature of the filament (Figure 11, right panel). They may lie along thin, dark strands that are part of the filament rather than the plage. Coherent, apparently upward motions are also detected at network boundaries along spicular-like structures. The most interesting results are at locations of diverging motions, as can be seen toward the upper end of the field (Figure 11). Some are associated with moderate flare-like brightenings (right panel in Figure 11 and Figure 10) and may suggest an explosive nature for these intensity changes. It is possible that some of the TR variability seen in TR lines with coarser resolution and attributed to stationary brightenings can actually be an effect of spatial smoothing of the above-mentioned flows. In other places, we find diverging vectors suggesting rotation. In the wavelet-processed movies, we see unwinding features at those areas. They are very suggestive of the so-called mini-coronal mass ejections detected recently by *Solar Terrestrial Relations Observatory* (STEREO) and associated with vortex flows at supergranular boundaries (Innes *et al.*, 2009).

A big advantage of VAULT's large FoV is the observation of similar structures both on disk and at the limb. The obvious candidates are the spicules. Koza, Rutten, and Vourlidas (2009) measured the dynamics of several Ly α spicules and found many similarities to the Hα dynamic fibrils despite the short VAULT time series. Based on the TRACE coalignment, we measure Ly α spicules to be $8'' - 12''$ in height, from VAULT spicule edge to the TRACE limb position. When we consider the co-aligned cotemporal BBSO Hα channel, Ly α spicules can be up to $\sim 2''$ higher than in the comparatively optically thinner Hα. Although scattered light may play a role in the ground-based observations, the height difference between Ly α and Hα appears to be significant. These results imply that Ly α spicules can be the outer sheaths of the Hα fibrils (Koza, Rutten, and Vourlidas, 2009). When we take into account similar results between Hα and C IV (de Wijn and De Pontieu, 2006) it becomes obvious that chromospheric mass is propelled to the corona *via* the fibrils and undergoes heating appearing in successively higher temperatures (Ly α to C IV, for example). This scenario seems to corroborate the very recent results of De Pontieu *et al.* (2009b), where it was proposed that Type II spicules may be the means of chromospheric plasma transport to coronal levels and temperatures and may play an important role in the coronal heating problem. Further observations of both fibrils and Type II spicules are, therefore, highly desirable in Ly α (in addition to chromospheric and coronal lines) to provide a more robust connection between the evolution of the chromospheric and coronal structures. For the moment, the preceding discussion suggests that spicules/fibrils may provide the mass heated to coronal temperatures (*e.g.*, de Pontieu *et al.*, 2007b).

Overall, our initial attempt to characterize the variability seen in the VAULT images seems to provide reasonable results. The most serious problem is the large amount of variability in all intensity and spatial levels. We plan to revisit the analysis of proper motions using our newly available wavelet-processed images that suppress the background "noise" and may enhance the effectiveness of cross-correlation techniques.

## 8. Discussion

The VAULT data, being taken from a sounding rocket platform, do not permit long time series investigations of the Ly α atmosphere. However, they do provide several tantalizing clues about the dynamics and morphology of the crucial interface of the upper chromosphere/lower TR, at least for long-lived structures and for variability at a time scale of a few minutes.

The improved photometric analysis of the VAULT data, combined with better Ly α models, shows that, for wideband imaging at least, most of the emission originates from the lower TR ($\geq 10^4$ K) and only the darker areas contain much chromospheric material (Table 2). Therefore, Ly α imaging observations are a great probe for the structure of the transition region (Teriaca *et al.*, 2005). It seems that the Ly α Quiet Sun is dominated by longer thread-like structures reminiscent of Hα fibrils. The VAULT observations provoked new ideas about the nature of the TR as the region where neutral hydrogen atoms from these threads diffuse across magnetic field lines, interact with nearby electrons, and subsequently excite, ionize, and/or radiate to provide the emission we see in TR lines (Judge, 2008). These ideas remain to be tested in detail, but they demonstrate the value of sounding rocket observations.

The high spatial resolution of the VAULT data resolves a great deal of variability, mostly associated with lateral motions, in the plage. We believe that the majority of this variability can be explained as buffeting of the Ly α structures by cooler material, such as Hα jets. In

addition, the VAULT observation of spicules show that they extend higher and have larger widths, but otherwise similar dynamics (Koza, Rutten, and Vourlidas, 2009) with their Hα counterparts. These observations verify past SUMER results (Budnik *et al.*, 1998) and provide significant support for an interesting idea put forth recently by de Pontieu *et al.* (2009a) to explain the large emission measure discrepancies between coronal and lower TR structures (Vourlidas *et al.*, 2001) as a result of extreme ultraviolet (EUV) absorption from chromospheric material injected in the corona. When we consider these observations and ideas together – namely, the long network loops and neutral cross-field diffusion, the continuous buffeting, and the Ly α jets as an extension of Hα dynamic fibrils – we come to the conclusion that the transition region may be nothing more than the transient, evaporating part of the chromosphere rather than the stable layer in the simple one-dimensional models, such as Vernazza, Avrett, and Loeser (1981), long favored in our discipline. The VAULT, and more recently, *Hinode*/SOT observations are making us reassess our views on the structure of the lower solar atmosphere.

The large field-of-view of the instrument led to observations of basically every solar structure, with the exception of coronal holes. This enabled us to estimate the contribution of various Ly α sources to the observed intensity and thereby introducing the first empirical segmentation of Ly α irradiance to its sources (Section 4). We find that Quiet Sun features can have intensities several times the intensity of the average Quiet Sun and that filaments exhibit both absorption and emission in Ly α. The latter can be as bright as weak bright points. Optically thin structures, up to 50% fainter than the average Quiet Sun, may exist in the center of cell interiors and as of-limb loops. We do find that high temperatures are likely in off-limb Ly α loops, which may explain their large heights ($\sim 60''$, corresponding to $\approx 45\,000$ km) in the VAULT images. We also find that active region filament partially absorbs plage emission, by around 20% to 30%, and this effect may need to be considered carefully in irradiance studies. These segmentation results may be useful to irradiance studies until full disk Ly α imaging becomes available.

The VAULT images provide the first ever unambiguous Ly α imaging of the fine structure of filaments/prominences and show that both emission and absorption takes place along the prominence backbone. It is interesting to note, that the underlying plage is visible through several locations along the prominence suggesting that Ly α is optically thin and that the distribution of hydrogen is highly anisotropic through these structures. It is also clear that the Ly α filament is larger than the Hα one (Millard, personal communication) and is likely to reach a higher altitude. The high LRI measurements in the filaments (up to 5, Table 2) are again consistent with a decreased optical thickness, even to the point of being optically thin. According to Gouttebroze, Vial, and Tsiropoula (1986) and their Figure 5, a very hot temperature of $\sim 5 \times 10^4$ K is also possible. For this study we chose the cooler more plausible solution of the curve. Nevertheless, with the lack of other observational constraints, it remains unsolved whether the hot solution is possible. One approach will be a point-to-point correlation with other chromospheric-TR lines. This calls for a high-resolution spectrograph, which is not currently available in space.

VAULT images also reveal a wealth of activity in both the plage and the Quiet Sun regions. In the latter, we see evidence of braiding in the loop structures outlining the cell boundaries. However, we do not see any direct unambiguous evidence of reconnection as will be expected from such activity. It may be that longer time series are needed to evidence such events. Alternatively, a mixture of cool absorbing structures propagating alongside these loops may create the appearance of braiding. Those structures may be the same absorbing structures that create the buffeting motions in the plage. On the other hand, we see frequent brightenings and even jets in the interior of the cells. This is the first time

that the Ly α emission from these areas was imaged and the amount of observed activity was unexpected. The brightenings seem to be associated with the emergence of magnetic field elements and their subsequent movement toward the cell boundary. These motions are regularly seen with subarcsecond resolution magnetographs [*e.g.*, Solar Optical Universal Polarimeter (SOUP) instrument; Title *et al.*, 1989], but we did not have any available during the flight. The relation between the emerging flux and the Ly α brightenings remains to be confirmed in a future flight; if it is true it suggests that the effects of even such small magnetic elements reach substantial heights in the solar atmosphere. We wonder whether some of those jets are the Ly α counterparts of the Type II spicules seen in the SOT observations (de Pontieu *et al.*, 2007b).

Another rather surprising observation is the relative scarcity of microflaring events. We are able to identify a handful in the five minutes of observation. These were previously identified by Berghmans, Clette, and Moses (1998). They suggested a possible link with atmospheric turbulence. In our observations, we observe them in both active regions and Quiet Sun regions. The largest of them has a light curve and energy consistent with a microflare and is detected in He II as well (Figure 9). Others have energies in the range of $10^{24}$ ergs. Although the short duration of the observation does not allow proper statistics for the occurrence of these events, our field-of-view covers a substantial part of the solar disk. Therefore, it seems unlikely that microflares are a common occurrence in this temperature range.

## 9. Conclusions

We conclude our overview of Ly α imaging observations with a set of "lessons learned" that may be useful in the design of future Ly α instruments or observation campaigns.

- Ly α is formed at the critical interface between the upper chromosphere and the low TR. Thus, imaging is very useful and the well-known difficulties surrounding the interpretation of Ly α emission are no longer insurmountable. We can rely on models to derive reasonable physical parameters for the observed structures.
- We see few Ly α structures close to the instrument resolution limit of 0.5″. Only absorbing (dark) features and off-limb structures (in emission) can be identified at that resolution. Most of the on-disk structures are much larger. This can be due to the high optical thickness of the line throughout these structures. In any case, this observation should be considered in the design of future Ly α telescopes. Extreme resolutions may not be useful unless the instruments can spectrally resolve the line or their science objectives include absorption or off-limb features.
- There is evidence of optically thin emission in many locations besides the obvious limb structures. Areas around filaments are especially interesting. This will require observations of the spectral profiles to be confirmed.
- There is considerable structure and variability within the cell interiors that is probably linked to photospheric flux emergence. This is a new area for Ly α studies and to understand it will require a future telescope sensitivity equal to or better than VAULT.
- Even if flaring activity is relatively unimportant, there is variability. Future instruments should achieve both high signal-to-noise ratio and cadence to allow the study of both.
- Both types of spicules are observable, and given the significant temperature range of Ly α formation, observations in Ly α are excellent tracers of the injection of material from the chromosphere to the corona.

For the near future, the advent of *Hinode*/SOT created a new and unique opportunity to address the nature of the transition region by combining VAULT and SOT observations of Quiet Sun structures and spicules. We plan to seek funding for refurbishment of the VAULT payload, which was damaged during its last flight, and for an underflight with SOT with the specific objectives of addressing the nature of the long Ly $\alpha$ fibrils over the quiet network and investigate Type II spicule dynamics, particularly at coronal holes. However, the dynamics of the Type I spicules and macro-spicules may need longer time series due to their longer lifetimes (Xia *et al.*, 2005).

To summarize, we present a broad overview of the morphology and dynamics of the Sun's Ly $\alpha$ atmosphere; an important, but rarely imaged region. These are the first sub-arcsecond, high sensitivity observations of this line, and at the time, the highest resolution observations of any solar structure from space. The VAULT observations show that Ly $\alpha$ emission arises from every location and in every solar feature, and generates new ideas about the nature of the transition region and coronal heating. These results demonstrate the wide ranging value of sounding rocket experiments despite their short observing windows.

**Acknowledgements** This work is dedicated to the memories of D. Prinz, G. Bruecker, and D. Lilley whose efforts contributed enormously to the success of the NRL sounding rocket programs. We are grateful to V. Yurchyshyn for providing calibrated BBSO H$\alpha$ images, and to J. Cook, J. Koza, S. Martin, R. Rutten, and J.C. Vial for useful discussion and constant encouragement. The achievements presented in this article are the product of many years of development work at the Naval Research Laboratory Solar Physics Branch and the NASA sounding rocket program. The VAULT instrument borrows heavily from the High Resolution Telescope and Spectrograph. The NRL rocket team of J. Smith, R. Moye, R. Hagood, R. Feldman, J. Moser, D. Roberts, T. Spears, and R. Waymire did a superb job in preparing and launching the instrument. We would like to acknowledge the efforts of the sounding rocket support team that made the VAULT launches possible. We would like to particularly acknowledge the following individuals. Tracy Gibb did a superb job managing the launch of the VAULT payload. Frank Lau managed the development of the Mark 7 digital SPARCS attitude control system. We would like to acknowledge the SPARCS team for their superb efforts in the support of our launch. Jesus and Carlos Martinez developed and operated the Mark 7 SPARCS. Richard Garcia, Shelby Elborn, and Kenneth Starr developed the VAULT telemetry section. The support from the White Sands Missile Range and Wallops Flight Facility NASROC personnel was of the highest caliber. The VAULT instrument development work was supported by the ONR task area SP033-02-43 and by NASA defense procurement request S-84002F. SOHO (EIT, MDI, and SUMER data) is a project of international cooperation between ESA and NASA.



## References

Antiochos, S.K., Noci, G.: 1986, *Astrophys. J.* **301**, 440.
Bartoe, J.D.F., Brueckner, G.E.: 1975, *Bull. Am. Astron. Soc.* **7**, 432.
Benz, A.O., Krucker, S.: 2002, *Astrophys. J.* **568**, 413.
Berghmans, D., Clette, F., Moses, D.: 1998, *Astron. Astrophys.* **336**, 1039.
Bonnet, R.M., Tsiropoula, G.: 1982, *Solar Phys.* **75**, 139.
Bonnet, R.M., Decaudin, M., Bruner, E.C. Jr., Acton, L.W., Brown, W.A.: 1980, *Astrophys. J.* **237**, L47.
Budnik, F., Schroeder, K.P., Wilhelm, K., Glassmeier, K.H.: 1998, *Astron. Astrophys.* **334**, L77.
Curdt, W., Tian, H., Teriaca, L., Schühle, U., Lemaire, P.: 2008, *Astron. Astrophys.* **492**, L9.
de Pontieu, B., Berger, T.E., Schrijver, C.J., Title, A.M.: 1999, *Solar Phys.* **190**, 419.
de Pontieu, B., Hansteen, V.H., Rouppe van der Voort, L., van Noort, M., Carlsson, M.: 2007a, In: Heinzel, P., Dorotovič, I., Rutten, R.J. (eds.) *The Physics of Chromospheric Plasmas* **CS-368**, 65.
de Pontieu, B., McIntosh, S., Hansteen, V.H., Carlsson, M., Schrijver, C.J., Tarbell, T.D., Title, A.M., Shine, R.A., Suematsu, Y., Tsuneta, S., Katsukawa, Y., Ichimoto, K., Shimizu, T., Nagata, S.: 2007b, *Publ. Astron. Soc. Japan* **59**, 655.

de Pontieu, B., Hansteen, V.H., McIntosh, S.W., Patsourakos, S.: 2009a, *Astrophys. J.* **702**, 1016.
De Pontieu, B., McIntosh, S.W., Hansteen, V.H., Schrijver, C.J.: 2009b, *Astrophys. J.* **701**, L1.
de Wijn, A.G., De Pontieu, B.: 2006, *Astron. Astrophys.* **460**, 309.
Dowdy, J.F. Jr., Rabin, D., Moore, R.L.: 1986, *Solar Phys.* **105**, 35.
Emerich, C., Lemaire, P., Vial, J.C., Curdt, W., Schühle, U., Wilhelm, K.: 2005, *Icarus* **178**, 429.
Engvold, O.: 1998, In: Webb, D.F., Schmieder, B., Rust, D.M. (eds.) *IAU Colloq. 167: New Perspectives on Solar Prominences* **CS-150**, 23.
Feldman, U.: 1983, *Astrophys. J.* **275**, 367.
Feldman, U.: 1987, *Astrophys. J.* **320**, 426.
Feldman, U., Dammasch, I.E., Wilhelm, K.: 2000, *Space Sci. Rev.* **93**, 411.
Feldman, U., Dammasch, I.E., Landi, E.: 2009, *Astrophys. J.* **693**, 1474.
Fontenla, J., Reichmann, E.J., Tandberg-Hanssen, E.: 1988, *Astrophys. J.* **329**, 464.
Fontenla, J.M., Avrett, E.H., Loeser, R.: 2002, *Astrophys. J.* **572**, 636.
Gouttebroze, P.: 2004, *Astron. Astrophys.* **413**, 733.
Gouttebroze, P., Vial, J.C., Tsiropoula, G.: 1986, *Astron. Astrophys.* **154**, 154.
Gunár, S., Teriaca, L., Heinzel, P., Schühle, U.: 2006, In: *SOHO-17. 10 Years of SOHO and Beyond* **SP-617**, 63.
Innes, D.E., Genetelli, A., Attie, R., Potts, H.E.: 2009, *Astron. Astrophys.* **495**, 319.
Judge, P.: 2008, *Astrophys. J.* **683**, L87.
Judge, P., Centeno, R.: 2008, *Astrophys. J.* **687**, 1388.
Korendyke, C.M., Vourlidas, A., Cook, J.W., Dere, K.P., Howard, R.A., Morrill, J.S., Moses, J.D., Moulton, N.E., Socker, D.G.: 2001, *Solar Phys.* **200**, 63.
Koza, J., Rutten, R.J., Vourlidas, A.: 2009, *Astron. Astrophys.* **499**, 917.
Krucker, S., Benz, A.O.: 1998, *Astrophys. J.* **501**, L213.
Landi, E., Feldman, U.: 2004, *Astrophys. J.* **611**, 537.
Langangen, Ø., Carlsson, M., Rouppe van der Voort, L., Hansteen, V., De Pontieu, B.: 2008, *Astrophys. J.* **673**, 1194.
Lemaire, P., Emerich, C., Vial, J.C., Curdt, W., Schühle, U., Wilhelm, K.: 2004, In: *35th COSPAR Scientific Assembly, COSPAR, Plenary Meeting* **35**, 510.
Lin, Y., Engvold, O.R., Wiik, J.E.: 2003, *Solar Phys.* **216**, 109.
Millard, A.A., personal communication.
Miller, S.C. Jr., Mercure, R., Rense, W.A.: 1956, *Astrophys. J.* **124**, 580.
Ofman, L., Wang, T.J.: 2008, *Astron. Astrophys.* **482**, L9.
Okamoto, T.J., Tsuneta, S., Berger, T.E., Ichimoto, K., Katsukawa, Y., Lites, B.W., Nagata, S., Shibata, K., Shimizu, T., Shine, R.A., Suematsu, Y., Tarbell, T.D., Title, A.M.: 2007, *Science* **318**, 1577.
Patsourakos, S., Gouttebroze, P., Vourlidas, A.: 2007, *Astrophys. J.* **664**, 1214.
Peter, H.: 2001, *Astron. Astrophys.* **374**, 1108.
Prinz, D.K.: 1974, *Astrophys. J.* **187**, 369.
Prinz, D.K., Brueckner, G.E.: 1977, *J. Geophys. Res.* **82**, 1481.
Purcell, J.D., Widing, K.G.: 1972, *Astrophys. J.* **176**, 239.
Puschmann, K.G., Sailer, M.: 2006, *Astron. Astrophys.* **454**, 1011.
Rutten, R.J., van Veelen, B., Sütterlin, P.: 2008, *Solar Phys.* **251**, 533.
Schrijver, C.J.: 2001, *Solar Phys.* **198**, 325.
Schrijver, C.J., Title, A.M., van Ballegooijen, A.A., Hagenaar, H.J., Shine, R.A.: 1997, *Astrophys. J.* **487**, 424.
Stenborg, G., Vourlidas, A., Howard, R.A.: 2008, *Astrophys. J.* **674**, 1201.
Teriaca, L., Schühle, U., Solanki, S.K., Curdt, W., Marsch, E.: 2005, In: Innes, D.E., Lagg, A., Solanki, S.A. (eds.) *Chromospheric and Coronal Magnetic Fields* **SP-596**, 66.
Title, A.M., Tarbell, T.D., Topka, K.P., Ferguson, S.H., Shine, R.A., SOUP Team: 1989, *Astrophys. J.* **336**, 475.
Trujillo Bueno, J., Shchukina, N., Asensio Ramos, A.: 2004, *Nature* **430**, 326.
Tsiropoula, G., Alissandrakis, C., Bonnet, R.M., Gouttebroze, P.: 1986, *Astron. Astrophys.* **167**, 351.
Vernazza, J.E., Avrett, E.H., Loeser, R.: 1981, *Astrophys. J. Suppl.* **45**, 635.
Vourlidas, A., Klimchuk, J.A., Korendyke, C.M., Tarbell, T.D., Handy, B.N.: 2001, *Astrophys. J.* **563**, 374.
Wilhelm, K.: 2000, *Astron. Astrophys.* **360**, 351.
Wilhelm, K., Curdt, W., Marsch, E., Schühle, U., Lemaire, P., Gabriel, A., Vial, J.C., Grewing, M., Huber, M.C.E., Jordan, S.D., Poland, A.I., Thomas, R.J., Kühne, M., Timothy, J.G., Hassler, D.M., Siegmund, O.H.W.: 1995, *Solar Phys.* **162**, 189.
Woods, T.N., Rottman, G.J., White, O.R., Fontenla, J., Avrett, E.H.: 1995, *Astrophys. J.* **442**, 898.
Xia, L.D., Popescu, M.D., Doyle, J.G., Giannikakis, J.: 2005, *Astron. Astrophys.* **438**, 1115.